Title
Iodo-Bromsulphalein-123I as a Liver and Bilary Scanning Agent

Author
Goris, Michael L

Publication Date
2023-09-06

Submitted To:
J. Nuclear Medicine

Iodo-Bromsulphalein-^{123}I as a Liver and Bilary Scanning Agent **

Michael L. Goris, M.D., Ph.D.*

Donner Laboratory

University of California

Berkeley, California

** This work was supported in part by the U.S. Atomic Energy Commission under the contract No. W-7405-eng-48, and the Bay Area Heart Research Association.

* "Aangesteld Navorser" of the Belgian National Foundation for Scientific Investigation (NFWO).

DISCLAIMER

Iodo-Bromsulphalein-^{123}I as a liver and biliary scanning agent.

Michael L. Goris, M.D., Ph.D.

Donner Laboratory, University of California, Berkeley, California

Introduction

To a large extent ^{99m}Tc has replaced ^{131}I as the devil-do-all for imaging in Nuclear Medicine. Lungs, Kidneys, and liver have been visualized with ^{99m}Tc-labeled agents. This is well explained by the physical compatibility between the gamma (Anger) camera and the isotope, even when physiological excellence is lacking. Specifically for the liver this may have been a loss, since not all the information physicians may seek is to be found in the spatial distribution of the reticular cells in the liver. A ^{99m}Tc-labeled parenchymatous cell tracer has not been developed yet.

Of the tracers processed by the functioning parenchymal cell, Rose Bengal labeled with ^{131}I (RB^{131}I), has been used most frequently. The kinetics are not simple (1), but there is ample evidence that parenchymal cell tracers can provide information unavailable from data obtained with labeled colloid. RB^{131}I does allow the differentiation between surgical and nonsurgical jaundice (2,3,4). In infants especially, the patency determination of the biliary pathways by nonagressive means may be beneficial (5) and has led to successful interventions in congenital defects (6). The specificity of the tracer for the liver cell has helped in the diagnosis of functional hepatomas (7).

Plasma retention curves for RB^{131}I have been used but are not disease specific (8). Sensitivity and specificity differences with Bromsulphalein have been found to be due to the measuring techniques or the dose injected (2,9).

^{131}Iodine-labeled tracers fall short when high resolution, high quality

images are expected with the gamma camera. The reasons are the restriction put on the dose of activity, the relatively low detection efficiency, and the collimation difficulties. For years, Prof. W. Myers (10) has pleaded the case of ^{123}Iodine, which decays by electron capture with a 13-hour half life and has 159 KeV photons with 85% abundance. While its physical characteristics compare favorably with those of ^{99m}Tc, it possesses the labeling characteristics of all iodine isotopes. The labeling technique must be rapid, however, because of the short half life, and it must have a high yield because of the current high cost of production of ^{123}I (about $45/mCi). Comparatively, the labeling of Rose Bengal is more time consuming (11) than the convenient method described by Suwanik and Tubis (12) for BSP. In this work, we hope to demonstrate how ^{123}I-BSP potentially combines the advantages of RB^{131}I and ^{99m}Tc-colloid in liver function and morphology evaluation.

Materials and Methods

1. Labeling: The Suwanik and Tubis method (12) was used with only slight modifications. In short, to a mixture of radioiodide, with no carrier added, of the desired activity, 0.1 cc of KI (2 mg/ml) and 0.1 cc of KIO_3 (2 mg/ml), one adds 0.3 cc of 1N HCl followed by 1 cc of BSP (Bromsulphalein^{R}, (Hyson, Westcott & Dunning, Inc.) (50 mg/ml). Subsequently, the pH is brought to 3 with HCl, the mixture shaken and allowed to stand at room temperature for 30 minutes. At the end of this time, the pH is brought to 6-7 with NaOH, and the mixture is collected in a syringe prefilled with 1 cc of AG1-X8 resin (100-200 mesh, chloride form, Gio-Rad. Laboratories). The syringe is agitated to mix the contents which are passed through a millipore disposable unit (Swinnex®-13, 0.22 µm, Millipore Corporation) into a multidose injection vial. For the mouse experiments, the label was ^{125}I and for the dog experiments ^{123}I. In all cases, the specific activity was at least 40 µCi/mg BSP.

2. Testing: The labeled tracer, ^{125}I-BSP, was injected intravenously into male Swiss mice, weighing between 27 and 34 gm. Blood samples were taken over an interval of 15 minutes. In one series, a mixture of ^{125}I-BSP and RB^{131}I (Robengatope®, Squibb & Sons) was injected for simultaneous annalysis and comparison of the kinetics of those tracers. The total amount of BSP and its iodinated derivative, I-BSP, injected was approximately 0.2 mg (7 mg/kg). The data were analysed for comparison according to a two-compartment model (Fig. 1). ^{123}I-BSP was injected intravenously in Beagle dogs (10 kg, either sex), and the distribution of the tracer followed with an Anger Camera. The activity ranged from 0.15 - 1.5 mCi and the total amount of BSP and I-BSP from 4 to 40 mg (0.4 to 4 mg/kg). In one case, the dog has been previously injected with a ^{99m}Tc-S-colloid (Tesuloid®, Squibb & Sons), and the two studies were compared. With the camera, the spectral separation was possible only by using the upper half of ^{123}I 159 KeV photopeak. This reduced the count rate from the previously administered technetium tracer by a factor of five.

In every case, a parallel hole (low energy) collimator was used until most of the activity was localized in the gall bladder. Subsequently, pictures of the gall bladder were taken with the pinhole collimator.

The camera was interfaced with a computer, as described by T.F. Budinger (13). Data were accumulated in histogram mode with frames of 15 seconds. Each study required at least one hour for completion, while a high count rate was needed for the quality of the static images to which the Tc-Colloid images were compared.

A square area circumscribed by the detector circumference was mapped into a 64 x 64 matrix. Polaroid pictures for the morphological evaluation were generated directly from the camera's CRT display, while the date accumulated by the computer were used for the generation of time functions from

rectangular regions of interest and for teletype display in one of the following modes: a) the original data, collected in 15-second frames, divided into 4096 matrix elements (64 x 64), are recombined by addition into frames of 1 minute (or longer, depending on the count rate) in any given experiment. Furthermore, this new frame is reduced to a 1024 matrix (32 x 32) by replacing four original matrix elements (in a two-by-two array) with one containing the average value. The reduced frame is printed out, coded from 10 (for the maximum value within the frame) to 0, in a linear fashion. b) the reduction to 32 x 32 frame was not performed, and a region of the frame was printed out in a logarithmic code where 10=100%, 5=10%, 0=1% of a preset value, a type of display allowing for the evaluation of spatial distribution changes in time over a larger range of values with two-digit symbols, although with smaller sensitivity than in linear scales.

Results and Discussion

1. Experiments in mice: The results for ^{125}I-BSP are summarized in Table I-a and for RB^{131}I in Table I-b. Using the compartmental assumptions of Fig. 1, one can compute from Q, the injected dose, and from In_1 In_2, the intercepts, and s_1, s_2, the slopes, the following physiological values: α_{12} (min^{-1}), the fractional turnover rate from the intra- to the extravascular pool, a function of the global mean capillary permeability for the tracer; fF (ml/min) the clearance of the tracer to the liver, expressed as the liver blood flow F multiplied by the extraction efficiency f; the intra- (V_1) and extravascular (V_2) distribution volumes of the tracer. Since only V_1 is sampled, V_2 is a virtual volume computed by using equilibrium assumptions. V_1 is not necessarily totally intravascular but mainly. Unless the data are of exceptional quality, that is with a relative random error smaller than 2%, the error made in the parameter estimation with this type of analysis is notoriously large

(14,15). Normalizing the data and pooling them before curve fitting did help, and the results of this are shown in Table II. The extraction efficiency was higher for ^{125}I-BSP, but so was the extravascular volume (V_2). Early, the computed fraction taken up by the liver was larger for BSP. Table III illustrates the early ratio between liver and non-liver activity (compartment 1 and 2). At later times, redistribution within the liver would prevent comparison with ^{99m}Tc-colloid scans. From the mice experiments, therefore, a significant improvement over RB^{131}I was expected, beyond those due to the physical characteristics of ^{123}I.

2. External detection: Beagle experiments. In Fig. 2-a and 2-b, liver images are shown with ^{99m}Tc-S-colloid and ^{123}I-BSP, respectively, that were performed sequentially on the same dog. Initially, the resolution was similar, as expected, even considering the lower target/non-target ratio for ^{123}I-BSP at that time (10 minutes post injection). A relatively high non-liver background was still present, as shown in Fig. 3 (a printout of the reduced 32 x 32 matrix) at 19 minutes post injection. At 120 minutes, most of the activity was in the gall bladder (Fig. 2-c), also shown with a pinhole picture (Fig. 2-d).

Time curves for heart, liver, and gall bladder are shown in Fig. 4.

Disappointingly, the non-liver activity (heart) did not reach values much lower than 50% of its initial value. A part of this may be explained by the increasing interference of scattered rays originated from higher energy radiation from an ^{130}I contaminant as increasing amounts of the tracer concentrated in the field of the camera. Thirteen minutes after injection, the departure of the gall bladder curve from the characteristics of the liver curve reflects gall bladder accumulation. This is also illustrated in Fig. 6 showing the time-distribution relation of the tracer in a logarithmic display.

Since the dog gall bladder, unlike that of man, is located in the center of the liver, its activity interfered more with the demonstration of the liver clearance than would be expected in humans.

An interesting view of the gall bladder is shown in Fig. 5.

Conclusion

Inasmuch as ^{123}I-BSP does indeed behave in a manner similar to RB^{131}I, it will furnish the same type of information otherwise not available from colloidal scanning agents. Since the isotope can be given in higher doses and is compatible with the Anger camera, pictorial information approaching the quality expected of ^{99m}Tc agents can be gained. The restriction lies in the relatively high non-target background and the interference of the contaminant. On the other hand, ^{123}I-BSP is shown to provide images of very high quality of the gall bladder.

Summary

BSP can easily be labeled with ^{123}I. The potential of this tracer, compared to ^{131}Rose-Bengal and ^{99m}Tc-labeled colloids, is discussed with reference to experiments on mice and dogs.

BIBLIOGRAPHY

1. Lushbaugh, C.C., Kretchmar, A., Gibbs, W., Liver function measured by the blood clearance of Rose Bengal-^{131}I: a review and a model based on compartmental analysis of changes in arm, blood, and liver radioactivity. Dynamic Clinical Studies with Radio Isotopes, edited by Kniseley, R.M., Tauxe, W.M., Anderson, E.B., USAEC Division of Technical Information 1964.
2. Nordyke, R.A., Surgical vs. non-surgical jaundice. Differentiation by a combination of Rose Bengal-^{131}I and standard liver-function tests. JAMA 194: 949-953, 1965.
3. Eyler, W.R., Schuman, B.M., DuSault, L.A., The radioiodinated Rose Bengal liver scan as an aid in the differential diagnosis of jaundice. Am. J. Roentgenol 94: 469-476, 1965.
4. Clark, J.S., Barret, P., Fonkalsrud, E.W., Diagnosis of obstructive jaundice. California Med. 112: 44-58, May 1970.
5. Sharp, H.L., Drivit, W., Lowman, J.T., The diagnosis of complete intrahepatic obstruction by Rose Bengal-^{131}I. J. Pediat. 70: 46-53, 1967.
6. Williams, L.E., Fisher, J.H., Courtney, R.A., Preoperative diagnosis of choledochal cyst by hepatoscintigraphy. New England J. Med. 283:85-86, 1970.
7. Shoop, J.D., Functional Hepatoma demonstrated with Rose Bengal scanning. Am. J. Roentgenol 107: 51-53, 1969.
8. Rosenthal, L., The application of colloidal radiogold and radioiodinated Rose Bengal in hepatobiliary disease. Am. J. Roentgenol 101: 561-569, 1967.
9. Uthgenannt, H., Dahl, P., Piening O: Vergleichende untersuchungen mit dem radio-Bengalrosa-und dem Bromsulphalein-test. Deutsche Med. Wchnschr. 91: 211-216, 1966.
10. Myers, W.F., Anger, H.O., Radioiodine-123. Ninth Annual Meeting of the Society of Nuclear Medicine. J. Nuclear Medicine 3: 183, 1962.

11. Hallaba, E., Raich, M., Photo-induced labelling of Rose Bengal with ^{131}I by ultra-violet radiation. Internat. J. Appl. Radiation & Isotopes 18: 533-535, 1967.

12. Suwanik, R., Tubis, M., A simplified method for the preparation of ^{131}I-labelled sulfobromophtalein. Internat. J. Appl. Radiation & Isotopes 19: 833, 1968.

13. Buddinger, T.F., Clinical and research quantitative nuclear medicine system symposium on medical radioisotopes scintigraphy, Monte Carlo, October 1972. IAEA/SM-164/161 (LBL-1328).

14. Myhill, J., Wadsworth, G.P., Brownell, G.L., Investigation of an operator method in the analysis of biological tracer data. Biophys. J. 5: 89-107, 1965.

15. Myhill, J., Investigation of the effect of data error in the analysis of biological tracer data. Biophys. J. 7: 903-911, 1967.

Table I-a

In the mouse experiments, the observations are activity per volume as a function of time in the intravascular compartment I. The data could be fitted by the function $In_1 e^{-s_1 t} + In_2 e^{-s_2 t}$. The correspondance with the solutions presented in Fig. 1 is found as follows:

$Q/(In_1 + In_2) = V_1$; $In_1/Q = I_1$; $In_2/Q = I_2$; $\alpha_{21} = I_1 s_2 + I_2 s_1$; $\alpha_{13} = s_1 s_2/\alpha_{21}$; $\alpha_{12} = s_1 + s_2 - \alpha_{13} - \alpha_{21}$; $fF = \alpha_{13} V_1$; $V_2 = \alpha_{12} V_1/\alpha_{21}$.

T_1 and T_2 are the half-lives corresponding to s_1 and s_2. From this computation procedure, it follows that the effect of error propagation will be very large for V_2, and larger for fF and α_{12} than for α_{21} and α_{13}. This is reflected in the wide variation of the parameters from different mice.

The values are printed beyond their last significant digit to allow the reader to check the computation without undue rounding errors.

Table I-b

The computation is the same as in Table I-a. The data were collected after a simultaneous injection of ^{125}I-BSP and RB^{131}I in mice 11 to 15, and the results should be compared to those of the corresponding mice in Table I-a.

Table II

The data are pooled after normalizing in regard to the sum of the intercepts $I_1 + I_2$. The value for V_1 is the average of the values found for the corresponding mice and tracers in Tables I-a and I-b. Group I is composed of mice 1 to 7 and group 2 of mice 11 to 15, on which the simultaneous determinations for ^{125}I-BSP and RB^{131}I were performed. Since the determinations were simultaneous for both tracers in group II, the difference between fF for ^{125}I-BSP and RB^{131}I are due to a larger extraction efficiency for the former.

Table III

In the mouse experiments, the intravascular compartment was the only one sampled, but the derivations shown under Table I-a allowed us to derive all the parameters defined in the model in Fig. 1. In this way, to the extent that the assumptions are valid, the kinetics of both tracers are completely defined. The activity in blood and tissue is the sum of the activity in compartment I and II and is equal to:

$$Q(I_1 - I_3)e^{-s_1 t} + (I_2 + I_2)e^{-s_2 t})$$

The activity of the liver is equal to:

$$\alpha_{13} Q \int_0^t (I_1 e^{-s_1 t} + I_2 e^{-s_2 t})dt.$$

Using the values found for group II in Table II and the fact that $I_3 = \alpha_{12}/(s_1 - s_2)$, while assuming that the injected amount is unity, allowed us to compute the expected values for intra- and extrahepatic activity. The ratio hepatic/extrahepatic is an estimate of the target-to-background ratio assuming equal volume distributions.

Table I-a

FITTING PARAMETERS AND DERIVED PHYSIOLOGICAL VALUES FROM THE PLASMA DISAPPEARANCE CURVES IN MICE

^{125}I-BSP

Mouse #	1	2	3	4	7	11	12	13	14	15
I_1	0.985	0.975	0.983	0.984	0.973	0.961	0.948	0.967	0.963	0.942
I_2	0.015	0.025	0.017	0.016	0.027	0.039	0.052	0.033	0.037	0.058
T_2(min)	9.40	8.80	12.4	15.0	15.0	9.50	9.00	10.5	18.0	11.2
T_1(min)	0.65	0.60	0.55	0.58	0.45	0.80	1.10	0.70	0.90	1.10
$s_2 min^{-1}$	0.074	0.079	0.056	0.046	0.046	0.073	0.077	0.066	0.038	0.062
$s_1 min^{-1}$	1.066	1.155	1.260	1.195	1.540	0.866	0.630	0.990	0.770	0.900
V_1ml	2.385	1.752	1.534	2.817	1.393	2.624	1.833	2.532	3.026	2.887
12	0.162	0.263	0.313	0.302	0.664	0.223	0.140	0.278	0.287	0.346
21	0.088	0.105	0.076	0.063	0.085	0.103	0.105	0.096	0.065	0.110
13	0.889	0.866	0.927	0.876	0.837	0.613	0.462	0.682	0.457	0.506
fFml/min	2.12	1.55	1.42	2.47	1.16	1.61	0.85	1.73	1.38	1.46
V_2ml	4.38	4.38	6.32	39.2	10.9	5.67	2.44	7.35	13.4	9.07

Table I-b

$RB^{131}I$, done simultaneously with BSP in mice Nos. 11 to 15 in Table I-a

Mouse #	11	12	13	14	15
I_1	0.892	0.981	0.869	0.889	0.797
I_2	0.108	0.119	0.131	0.111	0.203
T_2(min)	15.0	9.00	10.5	17.5	10.2
T_1(min)	1.10	1.50	1.15	1.35	1.60
$s_2 min^{-1}$	0.046	0.077	0.066	0.040	0.068
$s_1 min^{-1}$	0.630	0.462	0.603	0.513	0.433
V_1ml	2.070	2.108	2.520	2.456	2.499
12	0.300	0.032	0.240	0.238	0.152
21	0.108	0.084	0.136	0.098	0.141
13	0.268	0.423	0.293	0.223	0.209
fFml/min	0.55	0.89	0.74	0.55	0.52
V_2ml	5.75	0.80	4.45	6.35	2.68

Table II

FITTING PARAMETERS AND DERIVED PHYSIOLOGICAL VALUES FROM THE POOLED PLASMA DISAPPEARANCE RATE DATA

	Group I BSP	Group II BSP	Group II RB
I_1	0.978	0.954	0.850
I_2	0.022	0.046	0.150
T_2	10 min.	9.5 min	10.3 min
T_1	0.65 min	0.9 min	1.3 min
s_2	0.069 min^{-1}	0.073 min^{-1}	0.067 min^{-1}
s_1	1.066 min^{-1}	0.77 min^{-1}	0.533 min^{-1}
V_1	2.0	2.5	2.3
12	0.228	0.208	0.202
21	0.090	0.105	0.137
13	0.817	0.535	0.261
fF	1.634	1.337	0.600
V_2	5.1	4.8	3.4

Table III

DISTRIBUTION OF THE TOTAL DOSE BETWEEN LIVER AND NON-LIVER COMPARTMENTS (BLOOD+TISSUES) AT EARLY TIMES

	BSP			RB		
Time min.	Blood +Tissue	Liver	Ratio	Blood +Tissue	Liver	Ratio
0.	1.0	0.0	0.0	1.0	0.0	0.0
0.5	0.777	0.223	0.287	0.883	0.117	0.132
1.0	0.620	0.380	0.612	0.790	0.210	0.265
2.0	0.433	0.567	1.309	0.655	0.345	0.526
5.0	0.247	0.753	3.040	0.446	0.554	1.242
10.0	0.162	0.838	5.172	0.298	0.702	2.355

Fig. 1: Two-Compartmental Model for Bromsulphalein and Rose Bengal.

The analysis of the rate of change A_1 of the quantity of tracer present in compartment i is based on the following assumptions:

1) The tracer is restricted to compartments, I and II, between which there is exchange, and a third compartment, the liver, which acts as a sink.

2) In each compartment there is instantaneous mixing.

3) The kinetics are first order at all times.

4) The system is defined by the following constant values:

V_i is the volume of compartment i

f is the extraction efficiency by the liver

F is the blood flow to the liver

S is the average permeability multiplied by the area of the interface between compartment I and II

As shown in the figure, the rate of change $\dot{A}_1$ is due to the differences in concentration between compartment I and compartment II (C_2-C_1) multiplied by S, and the rate of liver uptake, fFC_1. The rate of change $\dot{A}_2$ is exclusively due to the concentration difference (C_1-C_2), multiplied by S.

The fractional turnover rates α_{ij} are defined as shown in the figure and represent the fraction of the tracer present in compartment going to compartment j per unit of time.

If Q is the amount initially introduced in compartment I, the solutions to the set of differential equations are $A_1(t) = Q(I_1e^{-s_1t} + I_2e^{-s_2t})$ and $A_2(t) = QI_3(e^{-s_2t} - e^{-s_1t})$. In terms of the fractional turnover rates α_{ij}, we have: $I_1 + I_2 = 1$; $I_1s_2 + I_2s_1 = \alpha_{21}$; $s_1 + s_2 = \alpha_{12} + \alpha_{13} + \alpha_{21}$; $s_1s_2 = \alpha_{13}\alpha_{21}$; $I_3(s_1-s_2) = \alpha_{12}$.

Fig. 2: Liver Imaging with ^{99m}Tc-S-Colloid and ^{123}Iodo-bromsulphalein.

In Fig. 2a, the ^{99m}Tc-S-Colloid image shows a defect in the center of the liver.

Only speculation as to the cause is possible. In Fig. 2b, the ^{123}I-BSP image is very similar to the one in Fig. 2a. However, the contrast was less pronounced due to the non-target background, and this is only partially corrected by photographic manipulation. In Fig. 2c, we have the image obtained 120 minutes after ^{123}I-BSP injection. Obviously the defect was due to a large central gall bladder. In Fig. 2d, a pinhole picture of the same gall bladder is shown. Note the lack of mixing in this very large (atonic?) gall bladder.

Fig. 3: Teletype Printout of a ^{123}BSP Liver Image.

The liver is the same as the one shown in Fig. 2. The data were originally collected in a 64 x 64 matrix, with integration time of 15 seconds. From this, frames of 60 seconds are generated by additions, and those are reduced to 32 x 32 frames by adding matrix elements (four matrix elements in two-by-two array), which allows us to print the frame on the teletype with two-digit symbols with minimal distortion. In this case, 10 stands for 1492 counts, and the scale is linear.

Fig. 4: Time Functions of Regional Activity over Heart, Liver, and Gall Bladder.

Those time functions are uncorrected for cross-talk, that is, the influence of scattered rays originating in one region, on the time function of another region. The liver time function includes the gall bladder time function. One has to remember that in external detection, the sampling is never pure and each curve represents a linear combination of activities originating in different subsystems. Hence, the heart curve is mostly due to intra- and extravascular activity (compartments I and II from Fig. 1) but, due to overlapping in the projection surface, may be influenced by liver and gall bladder activity. The liver curve contains a large element due to intra- and extravascular, but

extrahepatic activity. Due to a small change in position of the dog, between 30 and 40 minutes an artifact is more visible on the heart and gall bladder curves which were generated from smaller regions of interest than the liver one.

Fig. 5: Image of the Gall Bladder Obtained with ^{123}I-BSP.

Fig. 6: Time-Distribution of ^{123}I-BSP in a Dog.

In this display, the frames represent counts integrated over 1 minute, as in Fig. 3. However, the reduction to a 32 x 32 matrix was not performed. The code is logarithmic, in the four frames, 10 = 873 counts, 5 = 87, and 0 = 8. The heart, liver, and gall bladder regions are delineated to emphasize the distribution changes.

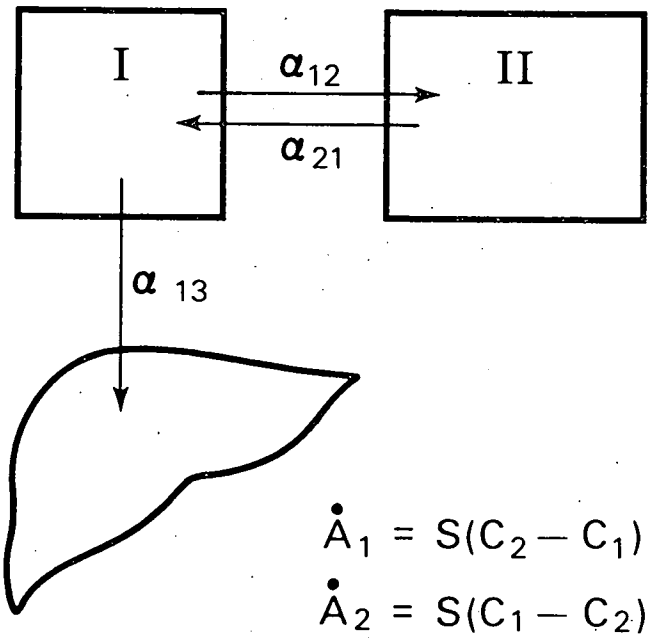

$$\dot{A}_1 = S(C_2 - C_1) - fFC_1$$

$$\dot{A}_2 = S(C_1 - C_2)$$

$$\alpha_{12} = S/V_1$$

$$\alpha_{21} = S/V_2$$

$$\alpha_{13} = fF/V_1$$

DBL 732-5050

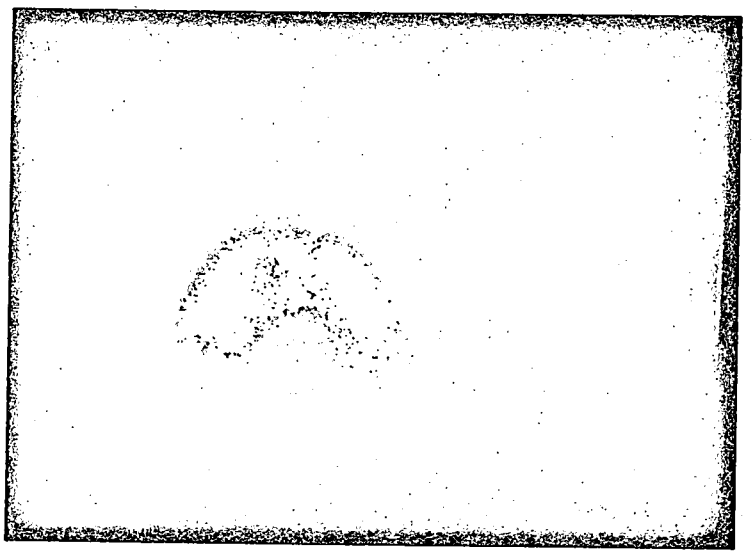

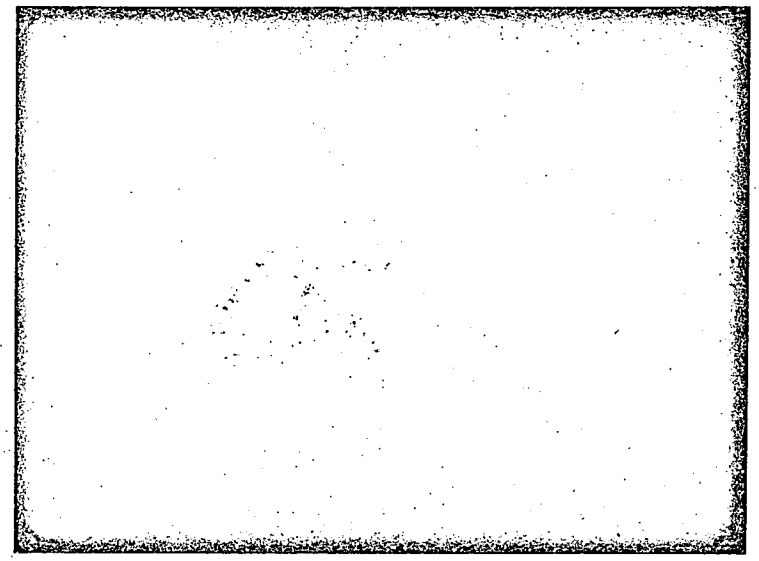

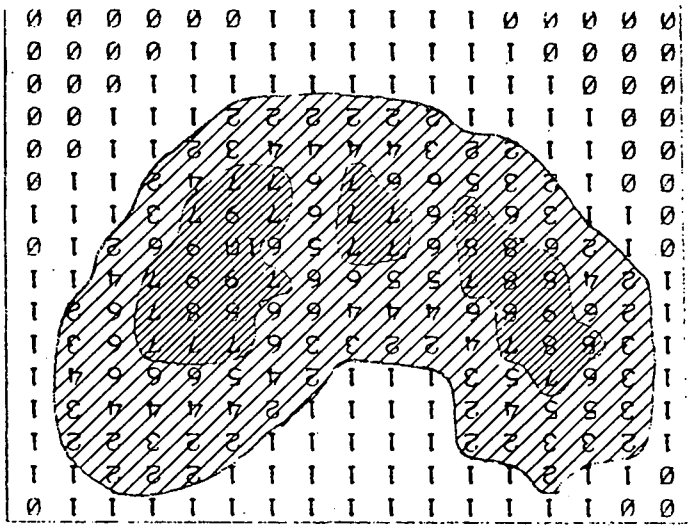

D2, ^{123}I-BSP, 19 min, 6000, 373

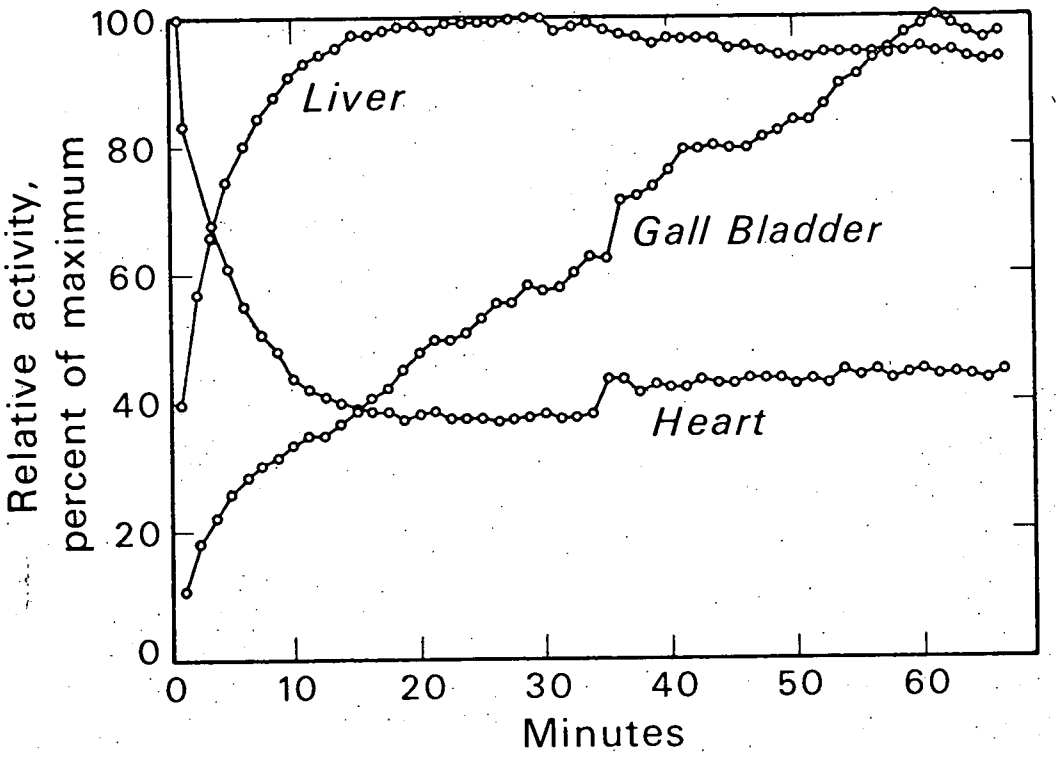
Relative activity, percent of maximum
100
80
60
40
20
0
0
10
20
30
40
50
60
Minutes
Liver
Gall Bladder
Heart

DBL 732-5052

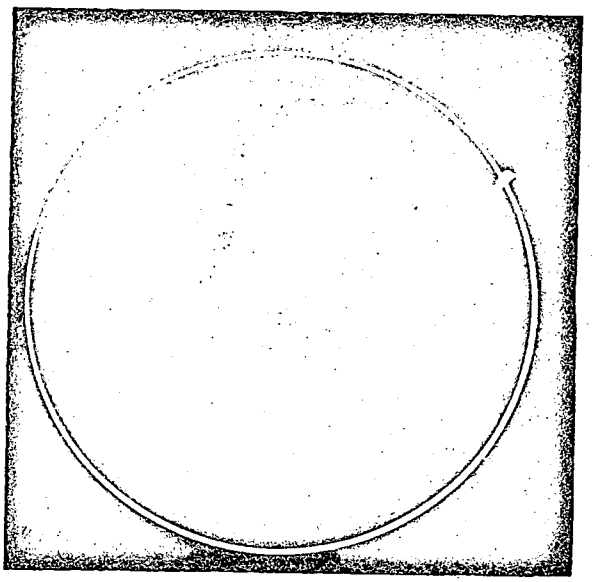

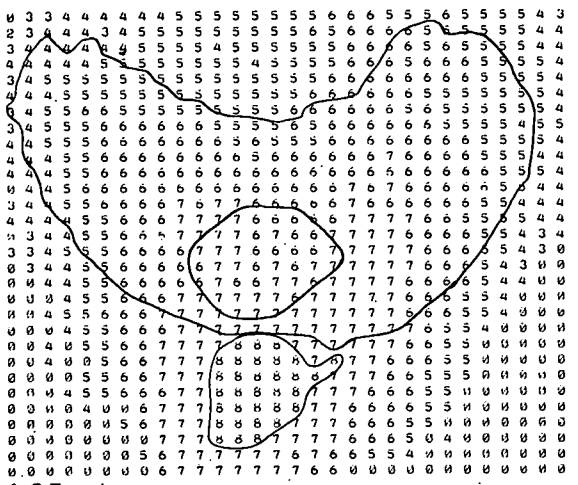

1.25 min

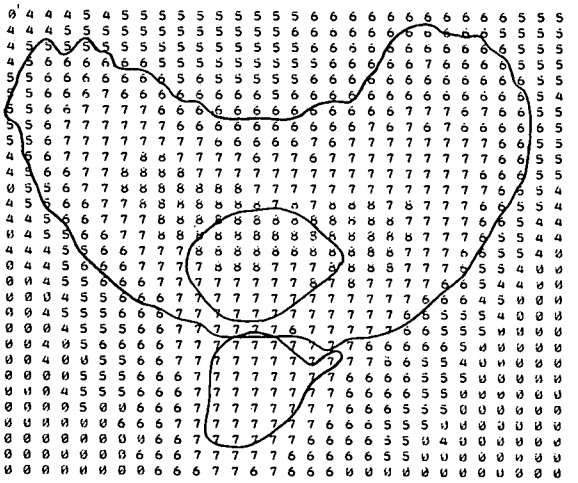

2.5 min

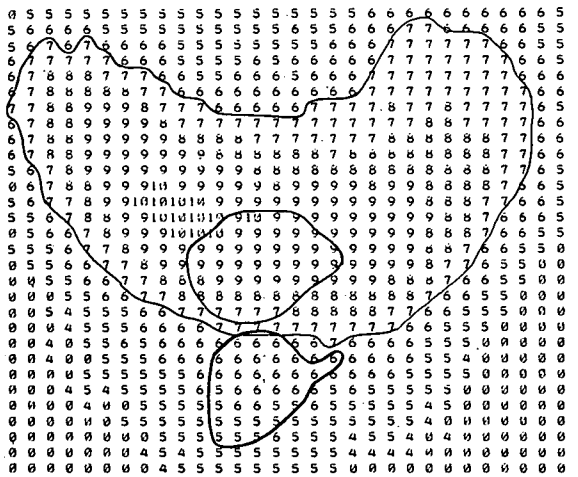

13.75 min

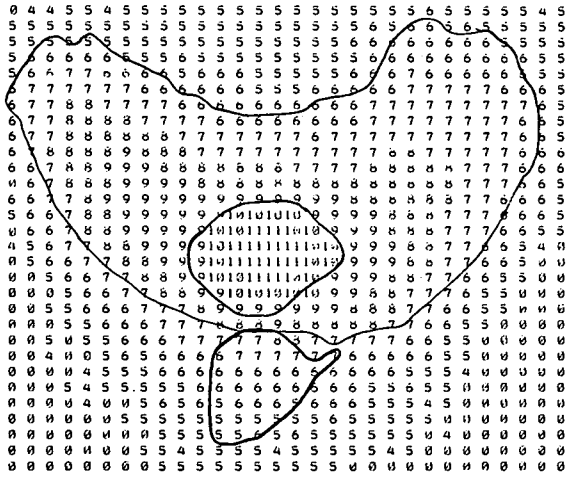

51.25 min

Loretta

For Patent review & number assignment

Bami

3/28

Special

LBL-1749

Bio-Med.